Droplet Sizing of electrospray based on Interferometric Laser Imaging

Hasan Rezaee[1], Azadeh Kebriaee[*]

[1]Aerospace Engineering Department, Sharif University of Technology, Tehran, Iran

*Corresponding author: kebriaee@sharif.ir

Abstract

Electrospray is applied to form very fine, small and monodisperse droplets using in pharmaceutical manufacturing, spaceship thrusters, and electrospinning. In this paper, the size distribution of electrospray in various modes has determined by Interferometric Laser Imaging for Droplet Sizing (ILIDS) technique. Bases on ILIDS method, droplets are irradiated by monochrome sheet laser, where the superposition of reflected and first-order refracted beams form a parallel fringe pattern at out of focus plane on the imaging sensor in the forward-scatter region. For the present work, an image processing algorithm is utilized to capture weak and noisy images of droplets to reduce the lost data in the sizing procedure. Since ILIDS method is applied for small and dilute spray, it is suitable for electrospray with Sauter Mean Diameter less than 20 microns. Two parameters including mass flow rate and applied voltage are considered as independent variables affecting on droplet sizing in the electrospray. Generally, our results confirm that a uniform distribution is formed in downstream of jet breakup in electrospray. The more populated region of spray is attributed to the axial zone near the point of breakup, where the unstable jet is disintegrated to droplets with larger diameters.

Keywords

Droplet sizing, Interferometric Laser Imaging, Electrospray

Introduction

In the field of spray analysis, one of the most important properties is the size distribution of droplets. Numerous techniques have been developed for sizing the droplets, e.g., shadowgraphy, Phase Doppler Anemometry (PDA), laser diffraction, interferometric laser imaging (ILIDS). Every technique has features that make the method suitable for a specific type of spray. For instance, diffraction measurements have no accurate spatial resolution while PDA has an excellent spatial resolution for time-averaged droplet-size distributions [1]. In principle, Imaging technique coupled with high-speed photography could provide both spatial and temporal information although the accuracy rapidly falls for small droplets (in the order of 10 μm or less). More magnifying could be a remedy to raise accuracy with a restricted field of view! ILIDS is an out-of-focus imaging technique which relies on interferometry providing instantaneous size and spatial distribution of transparent and spherical particles (droplets or bubbles) in a section of a flow with tolerable accuracy (better than 2% [2] [3]) for diameter range approximately from 2 to 200 μm [3], [4] and precise spatial resolution [1]. Also, it could be used to measure two components of velocity simultaneously. ILIDS was introduced by Konig et al. [2] and Ragucci et al. [4] These two groups used this method to measure the size of a single droplet. Then, Glover et al. [1] implemented the technique on a spray. They developed an out of focus imaging configuration which would make a fringe pattern on the image plane and used images data for sizing the droplets. The fringe pattern comes from the interference between external reflected and the first order of refracted ray scattered from the droplet in the forward region, also known as the glare points (see Figure 4).

van de Hulst [5] showed more than 99.5% of the total forward scattered light independent of incident light polarization composed of the first two orders of light and also hinted that for size parameter $x = \pi d/\lambda \gg 1$ geometric analysis can be useful. Glantschnig and Chen [6] approved that the first two orders of light rays require to consider for the interference analysis in geometric optics approach. The results match precisely with the exact solution of Lorentz-Mie theory. Also, they published a relation between the fringe angular spacing, the size parameter, the relative refractive index, and the scattering angle. Besides, Konig et al. [2] presented an equation which is simpler than the previous versions, but the independence of equation from the scattering angle makes the equation suitable in a more limited scattering angles. Therefore, Glantschnig's equation that republished by Hesselbacher et al. [3] is frequently applied by researchers. This equation is calculated as follows,

$$d = \frac{2\lambda N}{\alpha}\left(\cos\frac{\theta}{2} + \frac{m\sin\frac{\theta}{2}}{\sqrt{m^2 - 2m\cos\frac{\theta}{2} + 1}}\right)^{-1} \tag{1}$$

where d represents the droplet diameter, α is collecting angle, N is the number of fringes (α/N shows the angular fringe spacing), λ is the wavelength, m is the real part of the relative refractive index, and θ denotes the off-axis angle (scattering angle). This relation is not valid for scattering angle more than $82°$ and applicable up to $\sim 60°$ (for water, $m = 1.33$) [6]. Also, Hesselbacher et al. [3] investigated Gaussian beam effects on the accuracy of ILIDS method. They verified the precision of the technique in the presence of Gaussian beam effects for the laser sheet thickness larger than droplet diameter.

In the present work, we used ILIDS suitable for sizing small droplets to characterize electrospray. Over the past hundred years, electrospray applications have been increasing in industries like pharmaceutical manufacturing, spaceship thrusters, coloring and coating, agriculture and electrospinning [7]-[14]. The most important feature of electrospray is the fine and approximately monodisperse spray which make it more relevant for mentioned applications. In this work, the applied voltage changed from 4.2 to 5.0 kV and the volume flow rate varied from 1 to 4 mL/h. The fluid was ethanol. To validate the ILIDS method, we simultaneously used ILIDS and shadowgraphy setups to characterize the spray in three different volume flow rates. The principles and details of ILIDS are described in the following sections.

Principles of ILIDS

The interferometric laser imaging is based on the intensity distribution of scattered light from a single droplet (or bubble) in the forward scattering region. Figure 1 shows the intensity of scattered light as a function of scattering angle from a 10 µm ethanol droplet calculated with Mie scattering theory.

As seen in Figure 1, in the forward scatter region (around $20°$ to $80°$) there are regular fringes that arise from interference of all rays that leave the droplet with the same scattering angle θ [2], [6]. When a light ray reaches the surface of a droplet, a part of it reflected externally (called $p = 0$ or p_0). The rest of the light entered the droplet through refraction with a changing in the direction, calculated by Snell's law (Eq. 2) [2].
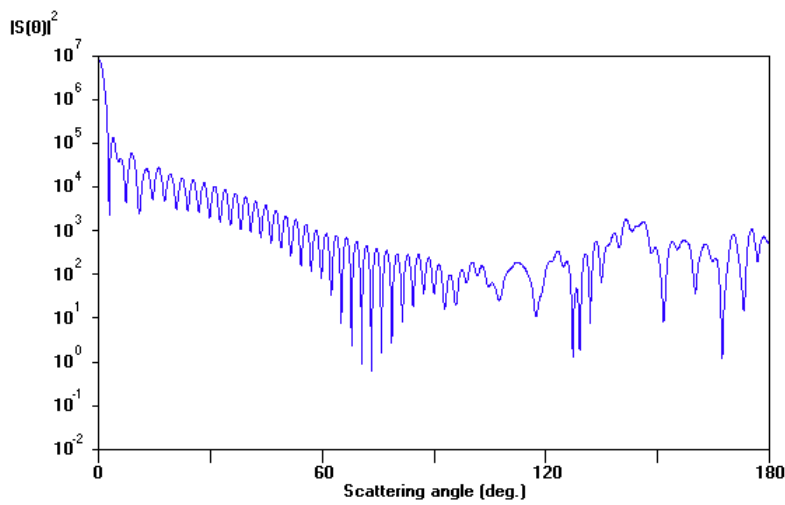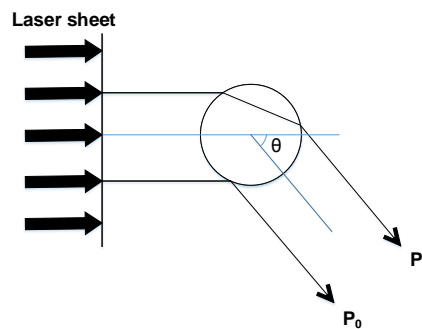

Figure 1. Intensity of light scattered from a 10 µm droplet illuminated by a 432 nm perpendicular polarized laser light

$$\sin(\tau') = \frac{1}{m}\sin(\tau) \tag{2}$$

Where τ and τ' are denoted in Figure 2 and m is the refractive index of the droplet. The refraction ray internally hits the front surface in the droplet, and the ray is divided into two rays, an internal reflection beam and a refracted ray leaving the droplet (called $p = 1$ or p_1). The intensity of a leaving ray depends on the incident light intensity, Fresnel's coefficients and divergence of the ray [1], [2]. This cycle continues until the intensity of the ray into the droplet falls to near zero. The light path through a droplet has been shown in Figure 2.
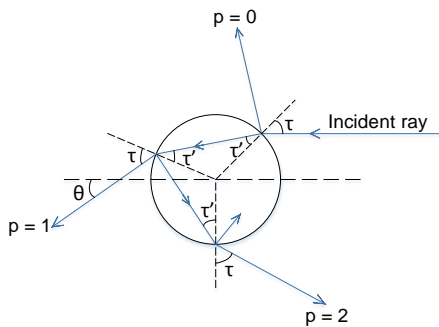

Figure 2. Path of an incident ray through a transparent spherical droplet.

Figure 3. Top view of two first order of light scattering from a droplet.

In the geometric optics the rays of order $p = 2$ and more could be neglected because the intensity of rays rapidly decreases with increasing order p [2], [5]. Glantshnig et al. [6] show the regular oscillations approximately comes from the interference of just externally reflected ray and the first order of refraction (p_0 and p_1). The schematic of these two first-order beams of light gathered by the lens is shown in Figure 3. These two rays are observed as the glare points if the droplet located in the focal plane. When camera moves away from the focal plane, these two glare points form bokeh shape and finally this two bokeh merge into one single image with interference pattern (see Figure 4) that created due to the optical path difference (OPD) and consequently phase shift between two rays of order $p = 0, 1$ [1], [6], [15], [16].

Angular spacing of these fringes depends on the setup configuration and the droplet diameter [6], Therefore, the droplet diameter is achieved by having the collecting angle and number of fringes.
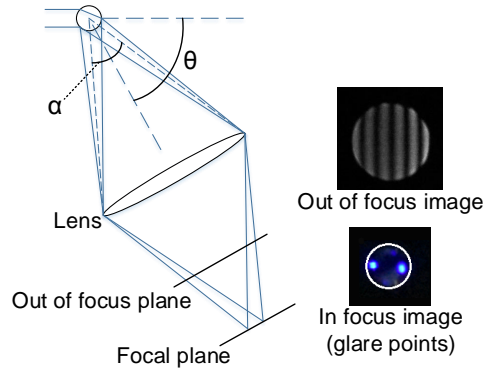
Figure 4. Schematic representation of how glare points and interferometric pattern are formed.

Setup configuration

A 432 nm cw laser light sheet with an approximate thickness of 1 mm was used to illuminate the ethanol electrospray droplets. The electrospray was formed by using a high voltage supplier and a syringe pump. The imaging device contained a 1.3 megapixel CMOS XIMEA-MQ013CG camera with USB 3.0 Interface with an AF Micro-Nikkor 200 mm f/4D ED lens. The experimental setup is depicted schematically in Figure 5. The exposure time was set equal to 15 μs. The needle material was stainless steel with the outer diameter and the inner diameter of 0.82 mm and 0.51 mm, respectively. The distance between the needle and the counter electrode was 50 mm. The counter electrode was a circular plate of aluminum with a diameter of 100 mm and 2 mm as thickness. Ethanol had a density of 789 kg/m^3, a viscosity of 1.1 mPa.s, a surface tension of 0.024 N/m, a conductivity of 7E-6 S/m, a dielectric constant of 24, and a refractive index of 1.3699. An external aperture with a diameter of 40 mm was located in 221 mm of test section which specifies collecting angle equal to $10.26°$. The scattering angle was $60°$ to get high visibility. The intensity of the reflected and the first order of refracted ray is approximately the same in this angle. The size of the measuring area was 4×4 mm^2. The grid of analyzed points started from 8 mm from needle to 20 mm and up to 10 mm in radius, as shown in Figure 6.
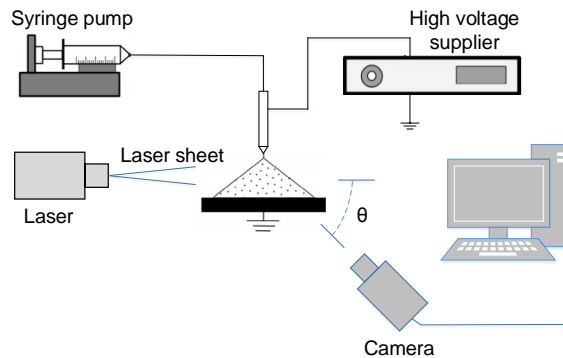
Figure 5. Schematic representation of experimental setup.

Validation and results

To validate the results of ILIDS method, this technique and shadowgraphy were simultaneously used to measuring the size of droplets in three different flow rates of 3, 6 and 9 mL/h for a constant applied voltage at 4.5 kV in an

electrospray setup. The comparison of the Sauter Mean Diameter (d_{32}) in Figure 7 represents a good agreement between shadowgraphy and ILIDS measurements. Since shadowgraphy technique is a proper method to sizing droplets down to the 10 μm, the measurement of the shadowgraphy technique is generally larger than ILIDS method. Results indicate that the difference between these two measurements methods is about 10% in the worst case related to larger droplets at high volume flow rate. It should be noted that ILIDS method is an appropriate method for tiny droplets and increasing the difference for a larger distribution of droplets could originate from omitting large droplets in ILIDS method.
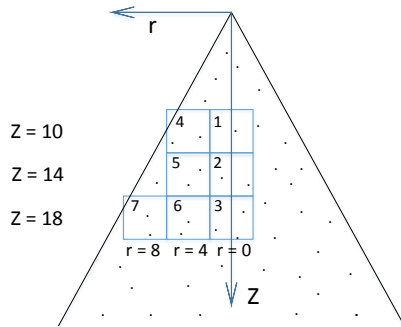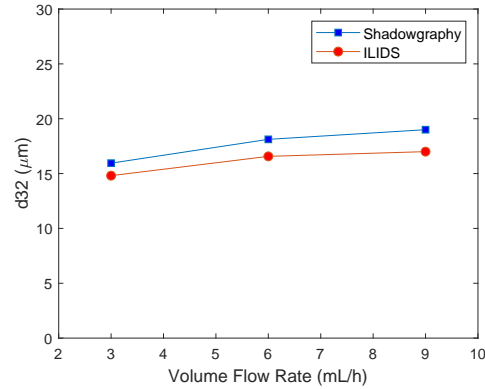

Figure 6. Analyzed grids.

Figure 7. Comparison of Sauter mean diameter obtained from shadowgraphy and ILIDS.

In the following section, the effects of applied voltage and flow rate are investigated on the Sauter mean diameter of an electrospray setup at different axial and radial positions of spray. Based on the authors' knowledge, the reports of ILIDS method are presented for the first time to sizing the droplets of an electrospray case in this work.

Effect of applied voltage in droplets size

The effects of the applied voltage in electrospray are analyzed on the droplets diameter, as shown in Figure 8. Every plot is attributed to a constant volume flow rate with variations of the applied voltage at 4.2, 4.5, 4.8, and 5 kV. Tests were examined for the volume flow rates of 1, 2, 3, and 4 mL/h at different axial and radial positions. The results are indicated for a region drawn in the axial direction from 16 mm to 20 mm and the radial direction from -2 mm to 2 mm (as depicted in Figure 6). The cumulative normalized volumetric distribution describes that the size of droplets diminishes with increasing the applied voltage. The reduction of the droplets size is more distinguishable for less volume flow rates, while an identical behavior is observed in the droplets size for the applied voltage of 4.5, 4.8, and 5 kV at Figure 8(c) and (d).

The enhancement of the electrical field at the spray region is the reason for decreasing the droplets size in the high applied voltage. In the high electrical field, the electrical force applied to the droplets raises and leads to accelerating the droplets.

Effect of volume flow rate in droplets size

Figure 9 shows the effects of volume flow rate on the size distribution of droplets at various applied voltages. The test section was the same as Figure 8. The different behaviors of this situation could be summarized as,

1. At low volume flow rate depicted by the solid blue line in the figures, the variations of applied voltage have an insignificant influence on the droplets size. Besides, it states that the change in droplets size is more recognizable in low volume flow rates(blue line) than the other higher volume flow rates for high applied voltage indicated in Figure 9 (d).

2. At moderate and high volume flow rates, a similar distribution of droplets size obtains for moderate voltages indicated in Figure 9 (b) and (c). While the size distribution of droplets is more sensitive to the volume flow rate in the range of 2-4 mL/h at low and high voltages shown in Figure 9 (a) and (d), respectively.

Size variations with changing modes

By surveying the breakup modes of electrospray, some relations between electrospray modes and droplets size distribution were deduced. Conditions mentioned above (applied voltage, flow rate, etc.) permit the electrospray to operate in three different modes. By using the shadowgraphy setup and imaging from the tip of the needle, these modes have been captured and presented in Figure 10. Figures 10(i), 10(ii) and 10(iii) show the cone-jet, spindle, and the oscillating-jet modes of electrospray, respectively. Besides, the mode variations by applied voltage and flow rate are depicted in Figure 9. Figure 9 shows the cone-jet mode has smaller droplets than the spindle or the unstable cone-jet. Thus, when electrospray operates in the cone-jet mode, increasing flow rate causing to form larger droplets.
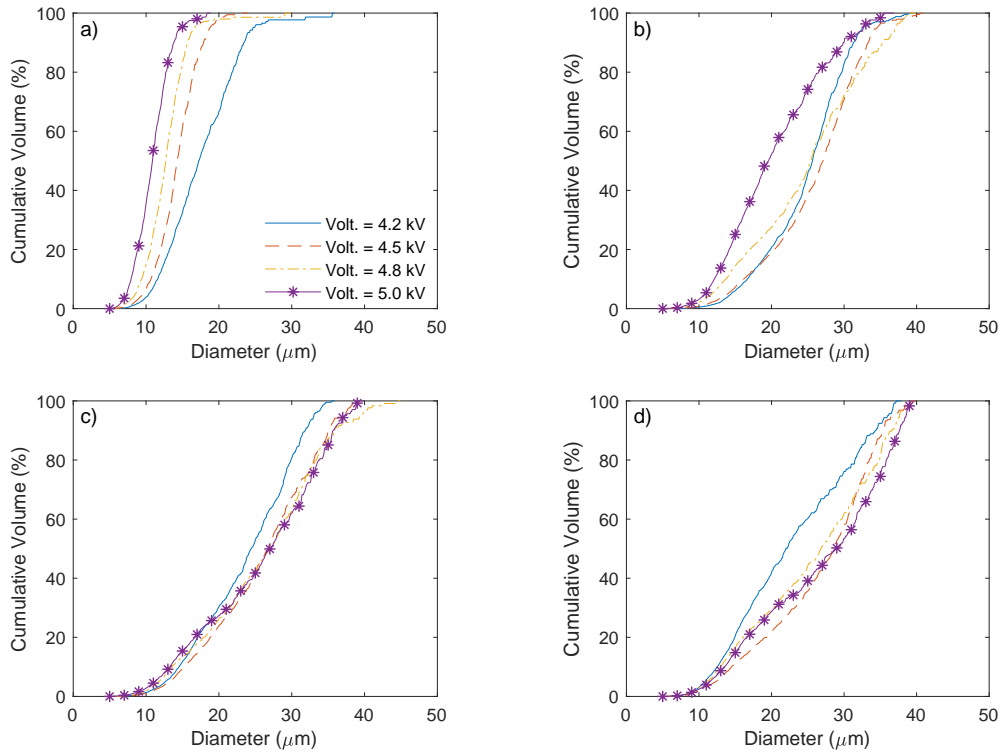
Figure 8. Effects of applied voltage on the cumulative volume versus diameter curve for volume flow rates of a) Q = 1 mL/h, b) Q = 2 mL/h, c) Q = 3 mL/h, d) Q = 4 mL/h.
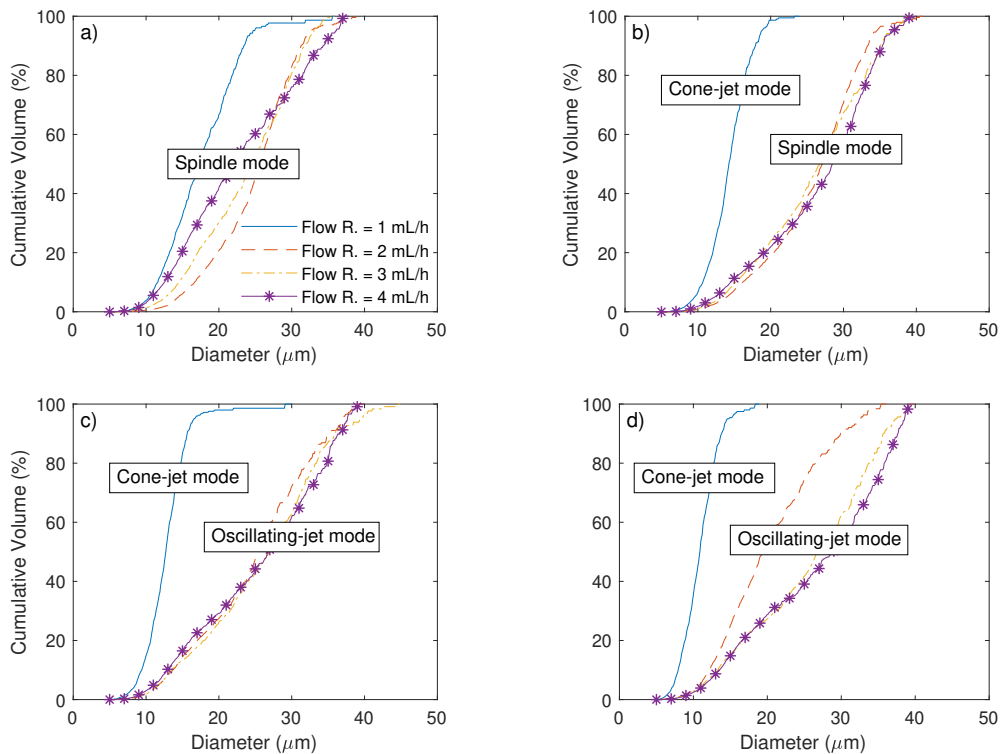
Figure 9. Effects of volume flow rate and the mode of electrospray on the cumulative volume versus diameter curve for applied voltages of a) V = 4.2 kV, b) V = 4.5 kV, c) V = 4.8 kV, d) V = 5 kV.

Axial and radial size distribution

According to the thermodynamic properties of Ethanol and the test ambient temperature (about $20°\,C$), the evaporation constant (K) obtained $\sim 1.69 \times 10^{-9}$ m^2/s. Using the D^2 *law* (Eq. 3) [17], for a 20 μm Ethanol droplet with velocity of 5 m/s (approximately velocity of droplets in analyzed modes of electrospray) the diameter reduction due
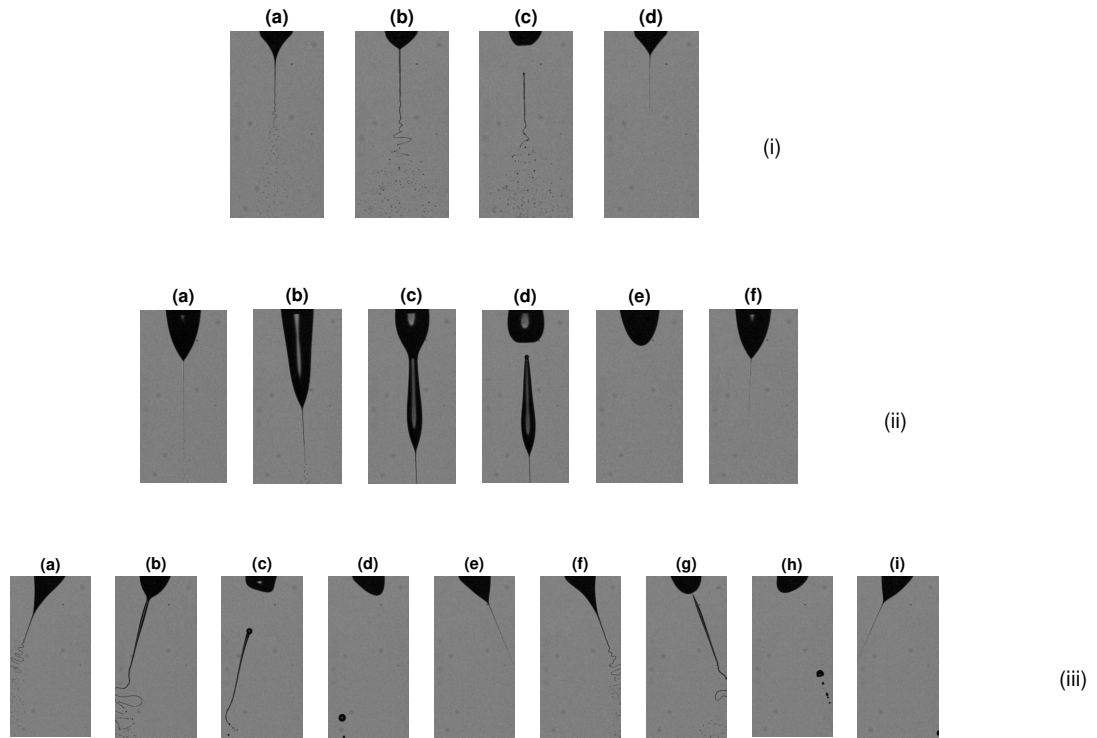
Figure 10. Cone-jet mode (i), spindle mode (ii) and oscillating-jet mode (iii) which happened under the test conditions.

to the evaporation is less than 0.9 μm, from z = 8 mm to 20 mm which is less than our resolution and is negligible!

$$D^2(t) = D_0^2 - Kt \tag{3}$$

The distribution of the droplets size in different regions of electrospray is illustrated in Figures 11 and 12. The Sauter mean diameter was calculated for different axial positions along the axis of the nozzle for various voltages and volume flow rates in Figure 11. The location of testing points changes from z = 8 mm to 20 mm down from the needle at r = 0 and 4 mm (grids 1, 2, 3 and 4,5,6 in the Figure 6). The Figure 11 is related to r = 0. Since the Weber number, defined as $We = \dfrac{\rho_l u_g^2 d}{\sigma}$, is in the low range in electrospray, the secondary atomization rarely occurs in the downstream of the spray flow. Therefore, a significant variation could not be observed for different axial positions especially for high volume flow rate indicated in Figures 11 (b)-(d). As known, there are some large size droplets in the axis of spray due to the Rayleigh-Taylor breakup of the jet. Because ILIDS method misses capturing such large droplets, the existence of some irregular patterns is inevitable in SMD diagrams. Results for the r = 4 mm was the same for r = 0.

In the Figure 12, SMD distribution is shown for different radial points from r = 0 mm to 10 mm at z = 18 mm (grids 3, 6 and 7 in the Figure 6). As depicted, a gradual decrement of d_{32} is explored by distancing from z-xis in electrospray. Similar to Figure 11, the variations in the droplets size is more distinguishable with changing the applied voltage for low volume flow rate in Figure 12(a) . The large droplets in Rayleigh-Taylor breakup could be the origin of larger SMD in r=0 while shooting the smaller droplets to further regions by whipping motions of the jet can lead to forming smaller SMD in larger radial locations. Also the radial size distribution analyzed at z = 14 mm and r = 0 mm to 6 mm (grids 2 and 5 in the Figure 6) and obtained the same result for z = 18 mm.

Conclusions

In this work, our focus was to develop the Interferometric Laser Imaging (ILIDS) method to determine the droplets size distribution in an electrospray. the main challenging problem to implement the ILIDS method was to identify the bright hashed region of droplets and enumerating the fringes for every droplet. A robust image processing code was written to measure the size of droplets with considering different approaches, e.g., recognizing the circular fringe pattern, extracting the level intensity, fast Fourier transform, and counting the peaks of level intensity. Finally, we used the ILIDS method to size the droplets in an electrospray setup. Our results confirmed that the secondary atomization rarely occurs for low-Weber number droplets in the electrospray. Also, distancing from the z-axis lead to having a smaller size distribution of droplets for different operational conditions. Findings indicated that enhancements in the applied voltage reduce the size of droplets while increasing the volume flow rate is accompanied by an increment in the size of the droplets.
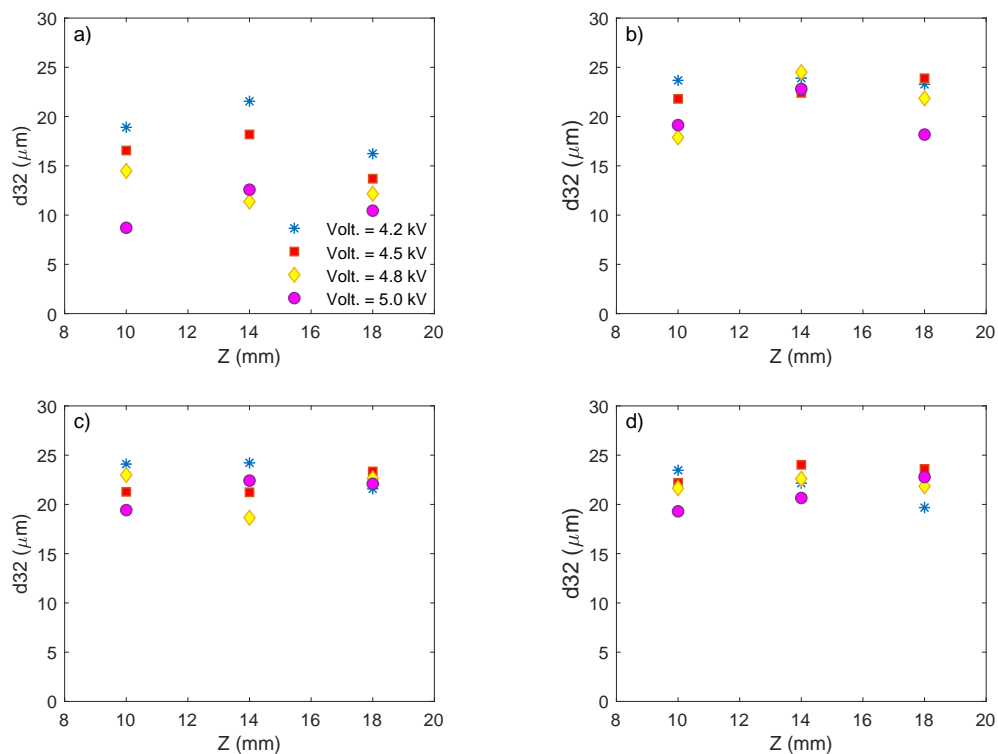
Figure 11. SMD variations in the axial direction for volume flow rates a) Q = 1 mL/h, b) Q = 2 mL/h, c) Q = 3 mL/h, d) Q = 4 mL/h.
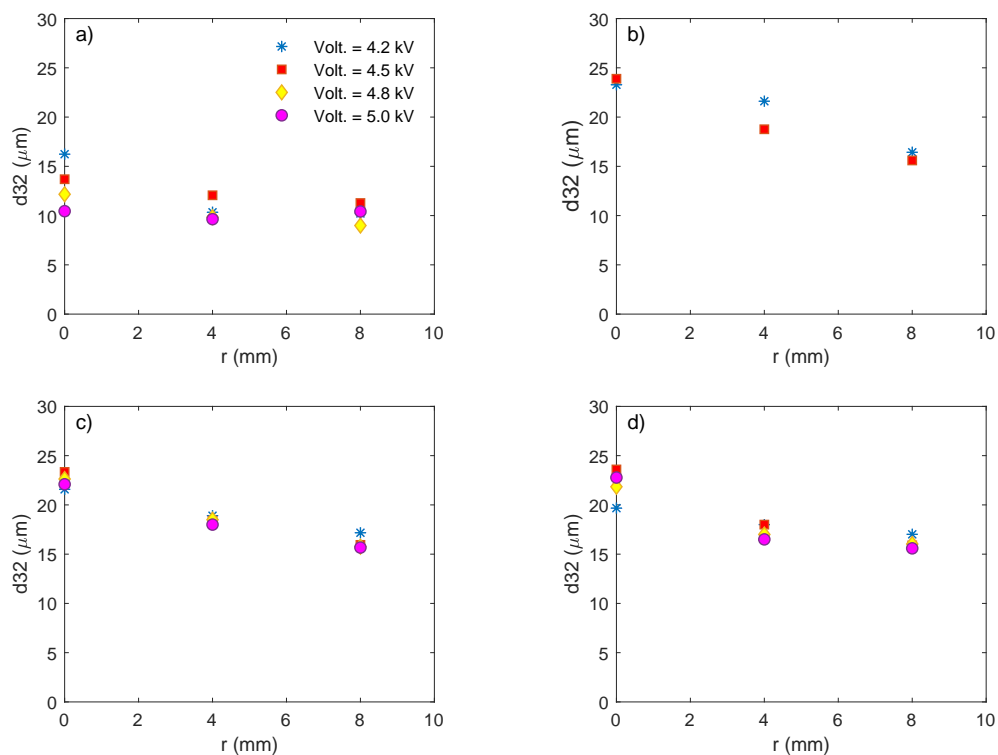

Figure 12. SMD variations in the radial direction for volume flow rates a) Q = 1 mL/h, b) Q = 2 mL/h, c) Q = 3 mL/h, d) Q = 4 mL/h.

Nomenclature

m	Refractive index [-]
Q	Volume flow rate [mL/h]
V	Voltage [V]
α	Collecting angle [radian]
λ	Wavelength [m]
θ	Scattering angle [radian]
τ	Angle of incident [radian]
τ'	Angle of refraction [radian]

References

[1] Glover, A. R., Skippon, S. M., Boyle, R. D., 1995, *Appl. Opt.*, 34, pp. 8409-8421.

[2] Konig, G., Anders, K., Frohn, A., 1986, *Aerosol Science*, 17, pp. 157-167.

[3] Hesselbacher, K. H., Anders, K., Frohn, A., 1991, *Appl. Opt.*, 30, pp. 4930-4935.

[4] Ragucci, R., Cavaliere, A., Massoli, P., *Part. Part. Syst. Charact.*, 7, pp. 221-225.

[5] van de Hulst, H. C., 1957, "Light Scattering by Small Particles". Dover Publications, Inc.

[6] Glantschnig, W. J., Chen, S. H., 1981, *Appl. Opt.*, 20, pp. 2499-2509.

[7] Seaver, A. E., Eckhardt, C. J., 1988, *US Patent*, 4,748,043.

[8] Hines, R., 1966, *Applied Physics*, 37 (7), pp. 2730-2736.

[9] Law, S. E., 2001, *Electrostatics*, 51, pp. 25-42.

[10] Jahannama, M., Watkins, A., Yule, A., Jul. 15.-17. 1999, 15th European Conference on Liquid Atomization and Spray Systems.

[11] Gamero-Castano, M., Hruby, V., 2001, *Propulsion and Power*, 17 (5), pp. 977-987.

[12] Grustan-Gutierrez, E., Gamero-Castano, M., 2017, *Propulsion and Power*, 33 (4), pp. 984-991.

[13] Tang, K., Gomez, A., 1994, *Aerosol Science*, 25 (6), pp. 1237-1249.

[14] Chakraborty, S., Liao, I. C., Adler, A., Leong, K. W., 2009, *Advanced drug delivery reviews*, 61 (12), pp. 1043-1054.

[15] Damaschke, N., Nobach, H., Nonn, T., Semidetnov, N., Tropea, C., Jul. 8.-11. 2002, 11th international Symposium on applications of Laser techniques to Fluid Mechanics.

[16] Lemaitre, P., Porcheron, E., Nuboer, A., Grehan, G., Aug. 27. – Sep. 1. 2006, 10th International Conference on Liquid Atomization and Spray Systems.

[17] Turns, S. R., 2012, "An Introduction to Combustion: Concepts and Applications, 3rd ed.". McGraw-Hill Companies, Inc.